

RESEARCH ARTICLE

Location of brachial plexus birth injury affects functional outcomes in a rat model

Raveena M. Doshi¹  | Monique Y. Reid^{2,3} | Nikhil N. Dixit¹  |
Emily B. Fawcett^{2,3} | Jacqueline H. Cole^{2,3}  | Katherine R. Saul¹ 

¹Department of Mechanical and Aerospace Engineering, North Carolina State University, Raleigh, North Carolina, United States

²Joint Department of Biomedical Engineering, University of North Carolina, Chapel Hill, North Carolina, United States

³Joint Department of Biomedical Engineering, North Carolina State University, Raleigh, North Carolina, United States

Correspondence

Katherine R. Saul, Department of Mechanical and Aerospace Engineering, North Carolina State University, 1840 Entrepreneur Drive, Campus Box 7910, Raleigh, NC 27695, USA. Email: ksaul@ncsu.edu

Funding information

National Institutes of Health, Grant/Award Number: R21 HD088893

Abstract

Brachial plexus birth injury (BPBI) results in shoulder and elbow paralysis with shoulder internal rotation and elbow flexion contracture as frequent sequelae. The purpose of this study was to develop a technique for measuring functional movement and examine the effect of brachial plexus injury location (preganglionic and postganglionic) on functional movement outcomes in a rat model of BPBI, which we achieved through integration of gait analysis with musculoskeletal modeling and simulation. Eight weeks following unilateral brachial plexus injury, sagittal plane shoulder and elbow angles were extracted from gait recordings of young rats ($n = 18$), after which rats were sacrificed for bilateral muscle architecture measurements. Musculoskeletal models reflecting animal-specific muscle architecture parameters were used to simulate gait and extract muscle fiber lengths. The preganglionic neurectomy group spent significantly less ($p = 0.00116$) time in stance and walked with significantly less ($p < 0.05$) elbow flexion and shoulder protraction in the affected limb than postganglionic neurectomy or control groups. Linear regression revealed no significant linear relationship between passive shoulder external rotation and functional shoulder protraction range of motion. Despite significant restriction in longitudinal muscle growth, normalized functional fiber excursions did not differ significantly between groups. In fact, when superimposed on a normalized force-length curve, neurectomy-impaired muscle fibers (except subscapularis) accessed regions of the curve that overlapped with the control group. Our results suggest the presence of compensatory motor control strategies during locomotion following BPBI. The clinical implications of our findings support emphasis on functional movement analysis in treatment of BPBI, as functional and passive outcomes may differ substantially.

KEYWORDS

brachial plexus, forelimb, gait, musculoskeletal model, rat model

1 | INTRODUCTION

Brachial plexus birth injury (BPBI) occurs in at least 1.5 of every 1000 live births.¹ It is most frequently caused by traction on the brachial plexus during difficult childbirth, injuring C5–C6 brachial plexus nerve

roots² and weakening or paralyzing the shoulder and elbow.³ While spontaneous neurological recovery does occur, 20%–30% of patients suffer from residual deficits in nerve and muscle function,⁴ and up to 33% of patients sustain permanent postural and osseous deformities.³ Presentation of injury can vary according to nerve injury location

relative to the dorsal root ganglion: more severe shoulder and elbow contractures present with nerve root ruptures distal to the ganglion (postganglionic),⁵ while avulsion injuries proximal to the ganglion (preganglionic) typically present as paralysis without contracture.⁶ Postganglionic injuries demonstrate greater spontaneous recovery and amenability to surgical repair compared with preganglionic injuries.⁷

Rodent models are an established model for studying pathomechanics of BPBI; humans and rodents share similar shoulder anatomy and brachial plexus innervation,⁸ and surgically induced brachial plexus injury in rodents reproduces the musculoskeletal deformities and shoulder contracture observed in humans.⁹ Specifically, rodent models of BPBI exhibit impaired longitudinal muscle growth,⁹⁻¹² glenohumeral deformation,^{11,13} and shoulder internal rotation and elbow flexion contracture.^{5,9-13} Within injury types, rat models of BPBI demonstrate restricted longitudinal muscle growth of pectoralis major, spinal deltoid, and subscapularis following postganglionic injury and of spinal deltoid, biceps long head, biceps short head, supraspinatus, and teres major following preganglionic injury.¹²

While effects of BPBI on passive movement in rodent models have been documented, effects on functional movement remain underexplored, perhaps because of the difficulty associated with measuring functional movement parameters in vivo. Passive shoulder and elbow range of motion (ROM) have been evaluated in rodent models of BPBI under sedation and postmortem.^{5,10-13} Insight into the impact of BPBI on functional movement outcomes in rodent models can be beneficial in assessing effectiveness of therapies and surgical interventions currently employed in clinical treatment of infants. Furthermore, investigating the fidelity with which passive outcomes can predict functional performance in rodents may increase utility of passive performance data and elucidate mechanisms contributing to neuromotor and musculoskeletal deficits. Existing literature on functional movement following BPBI in rodent models includes qualitative reports of altered forelimb posture following preganglionic⁸ and postganglionic injury,¹³ and quantitative stride and stance metrics following postganglionic injury.¹⁴ The quantitative effects of injury location on functional limb posture and muscle excursion have not been previously studied.

Two potential useful tools for studying functional movement *ex vivo* are gait analysis and musculoskeletal modeling. Gait analysis can be an effective function-based quantitative method for studying BPBI in a rat model.¹⁴ Musculoskeletal models provide a framework for integrating anatomical and physiological data, offering insight into the biomechanics underlying movement. While upper-extremity models have been developed for the human,^{15,16} and one hindlimb model has been developed for the rat,¹⁷ the rat forelimb remains unmodeled. Coupled with gait analysis, musculoskeletal modeling and simulation offer insight into functional movement parameters such as muscle excursion that cannot be easily measured in vivo. In this study, we developed a noninvasive framework integrating musculoskeletal modeling with gait analysis to examine the effect of BPBI on functional movement. Specifically, we developed a musculoskeletal model of the rat forelimb using measured muscle architecture parameters and we simulated locomotion using limb posture from gait analysis to examine the effect of injury location on gait characteristics and muscle fiber

excursion. We hypothesized that injury location (preganglionic or postganglionic) would impact key characteristics of functional movement. We also hypothesized that previously measured passive ROM capabilities would be good predictors of functional performance.

2 | METHODS

The following procedures were approved by the Institutional Animal Care and Use Committee at North Carolina State University. We studied 18 Sprague Dawley rat pups that underwent surgical intervention 3–5 days postnatally as part of larger, prior studies. Details of the intervention are available in the prior publications.^{12,18} Briefly, animals received one of three unilateral surgical interventions: preganglionic neurectomy, postganglionic neurectomy, or sham surgery. Preganglionic neurectomy was performed through supraclavicular incision and excision of C5–C6 nerve roots proximal to the dorsal root ganglion. Because this procedure involves limited visual access to the nerve, success was determined through observation of an internally rotated and adducted limb within 24 h of surgery.^{5,12} Nerve roots were more easily visualized during postganglionic neurectomy, which was performed through transverse infraclavicular incision and splitting of the pectoralis major, and excision of C5–C6 nerve roots distal to the dorsal root ganglion.^{11,12} Eight weeks postoperatively, these rats participated in the assessment of maximum passive shoulder external rotation ROM and gait analysis. This time point corresponds to approximately 5.3 years of postnatal human musculoskeletal development,¹⁹ by which time shoulder deformity is well-established clinically. After gait analysis, rats were sacrificed, and bilateral muscles crossing the shoulder were dissected to characterize muscle mass, muscle belly length, and sarcomere length in a fixed posture: elbow flexed 90° and shoulder adducted and protracted neutrally. In this study, we examined the effect of nerve injury location on functional movement using gait analysis to determine limb posture during locomotion and a musculoskeletal model to extract fiber lengths. We studied the unimpaired limb of the sham surgery group as a control ($n = 6$) and the impaired limb of preganglionic ($n = 6$) and postganglionic ($n = 6$) neurectomy groups.

2.1 | Muscle architecture

We report new measures of architectural parameters necessary to compute muscle force-generating capacity. Muscle fiber length was measured using a digital caliper (0.01 mm accuracy) by isolating fiber bundles from muscles. Optimal fiber lengths (l_o^F) were calculated by normalizing measured fiber lengths (l^F) to a sarcomere length (l^S) of 2.4 μm , the optimal sarcomere length of rat skeletal muscle²⁰:

$$l_o^F = l^F \left(\frac{2.4}{l^S} \right). \quad (1)$$

Physiological cross-sectional area (PCSA) was calculated based on muscle mass (m^M), pennation angle (θ), and the density (ρ) of

mammalian muscle ($0.001056 \text{ g}\cdot\text{mm}^{-3}$)²¹ according to Sacks and Roy²²:

$$\text{PCSA} = \frac{m^M \cdot \cos\theta}{\rho \cdot l_o^F}. \quad (2)$$

Estimates of PCSA and specific tension (σ) of muscle (50.8 N/cm^2)²³ were used to calculate maximum isometric muscle force (F_o^M):

$$F_o^M = \text{PCSA} \cdot \sigma. \quad (3)$$

2.2 | Gait analysis

Rats were recorded walking on a treadmill (Exer-3/6, Columbus Instruments) with no incline at 5 m/min for 2 min.^{24,25} The camera was placed level with the center of the treadmill and oriented to capture sagittal plane movement. Before gait analysis, rats were acclimated to the treadmill over 2 days. Gait data were collected during a single assessment 8 weeks postoperatively with researchers blinded to group allocation. While some animals required nudging to initiate walking when first placed on the treadmill, no animals required incentives to walk during the gait cycles selected for this analysis, or in those immediately preceding and following selected cycles. A single gait cycle (from heel-strike) that included two heel-strikes and a toe-off immediately followed by a swing phase was chosen from each recording. Sample size for this study ($n = 6$ per group) was determined by the subset of animals from larger, prior studies^{12,18} that exhibited at least two consecutive cycles to ensure that continuous gait was achieved. Selected gait cycles were processed at 30 frames/s. Duty factor was calculated as the time from heel-strike to toe-off divided by total gait cycle duration,²⁶ representing the fraction of the gait cycle spent in stance by that limb. Sagittal plane shoulder and elbow angles were extracted by placing virtual markers on bony landmarks on the wrist, elbow, shoulder, and body midline (Figure 1) using Tracker. Shoulder angle (shoulder protraction hereafter) is the included angle between the midline and a line connecting the shoulder and elbow marker; a negative value for this rotation is equivalent to shoulder flexion in humans. Elbow angle (elbow flexion hereafter) is supplementary to the included angle between the shoulder, elbow, and wrist; a positive rotation is equivalent to elbow flexion in humans. To eliminate high frequency noise, a first-order Butterworth filter with a cut-off frequency of 6 Hz was implemented in MATLAB (The MathWorks).

2.3 | Musculoskeletal model

We developed 18 musculoskeletal models in OpenSim^{27,28} (v3.3, Stanford University) using animal-specific muscle parameters for the six rats from each group. Because animal-specific parameters were integrated into modeling for animal-specific analyses, researchers could not be blinded to group allocation during modeling and

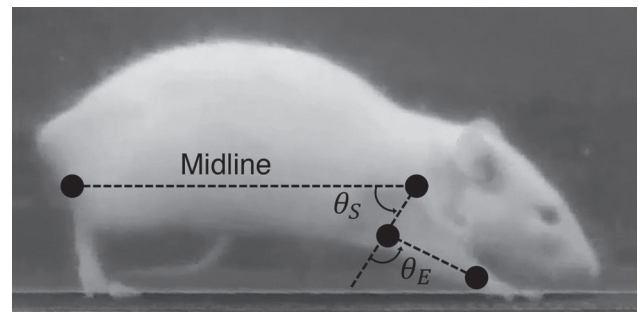


FIGURE 1 Sagittal plane joint angle tracking. Virtual markers, placed on bony landmarks of the wrist, elbow, shoulder, and body midline were used to track sagittal plane joint angles. Shoulder protraction (θ_S) is the included angle between the midline and a line between the shoulder and elbow markers. Elbow flexion (θ_E) is the supplementary angle to the included angle between the shoulder, elbow, and wrist

simulation. A generic skeletal structure was derived from publicly available microcomputed tomography (micro-CT) scans of a healthy, young (10-12 week-old) Sprague Dawley rat skull, spine, and unilateral scapula, humerus, forearm, clavicle, and hand.²⁹ Fourteen Hill-type muscle-tendon actuators were used to represent 10 muscles crossing the shoulder (pectoralis major, anterior deltoid, spinal deltoid, biceps long head, biceps short head, subscapularis, supraspinatus, infraspinatus, teres major, and triceps long head). Hill-type actuators determine muscle force production based on muscle activation level, length, velocity, and four major architectural parameters: maximum isometric force, optimal fiber length, tendon slack length, and pennation angle at optimal fiber length.³⁰ Maximum isometric forces and optimal fiber lengths were defined from individual anatomical measurements. Tendon slack length, which cannot be measured directly, was estimated such that muscle fiber length matched the value measured in the fixed posture during muscle dissection. Pennation angle at optimal fiber length was zero, as this parameter has little effect on PCSA in the rat forelimb.³¹ Muscle attachment locations and muscle paths were prescribed based on anatomical descriptions from literature.^{32,33} For muscles represented using two Hill-type actuators to span the shoulder (pectoralis major, anterior deltoid, spinal deltoid, and subscapularis), each actuator had half the reported maximum isometric force, such that muscle totals matched reported values.

Joint kinematic definitions including axes and degrees of freedom were defined based on standard veterinary anatomical conventions for quadrupedal mammals.³⁴ The shoulder joint coordinate system was placed at the glenohumeral joint (Figure 2). Protraction and retraction refer to cranial and caudal rotation of the humerus, respectively, about an axis pointing from the lateral to the medial face of the humeral head. Movements ventral to the zero position of this rotation are negative to indicate that the humerus is moving below the body axis.²⁹ Adduction and abduction refer to medial and lateral rotation, respectively, about an axis pointing from the ventral to the dorsal face of the humeral head. Internal rotation and external

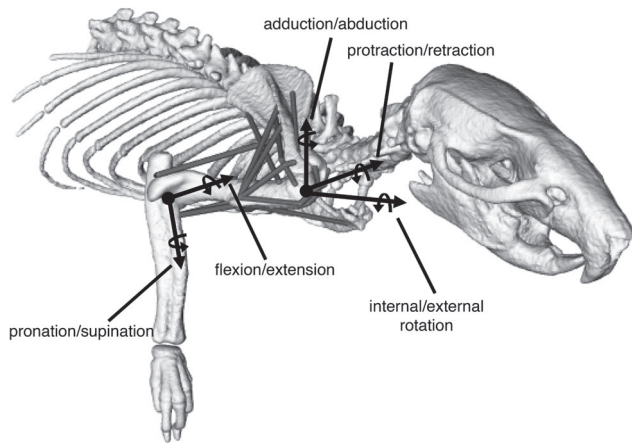


FIGURE 2 Degrees of freedom and axes of rotation are defined according to veterinary standards.³⁴ Shoulder degrees of freedom describe rotation of the humerus including protraction, adduction, and internal rotation. Elbow degrees of freedom describe rotation of the radius-ulna segment (coupled as the forearm) including flexion and pronation. Sagittal plane joint angles from gait analysis (Figure 1) map to protraction of the shoulder (θ_S) and flexion of the elbow (θ_E) in the musculoskeletal model

rotation describe medial and lateral rotation of the humerus, respectively, about an axis orthogonal to the two former axes. The elbow joint coordinate system was located between medial and lateral epicondyles of the humerus. Flexion and extension describe rotation of the forearm about an axis pointing from the medial to lateral epicondyle. Pronation and supination describe the rotation of the forearm about an axis pointing from the olecranon process to the midpoint of the radial and ulnar styloid processes.

To validate the musculoskeletal model, simulations of passive external rotation ROM were compared with experimental values from the prior report.¹⁸ The shoulder was rotated externally from 0 to 90°, and the moment generated by a single muscle was calculated as the muscle-tendon force times the moment arm at each joint angle. ROM endpoint was defined as the joint angle at which muscles crossing the shoulder exerted a net passive force sufficient to restrict external shoulder rotation against a 10-g load applied at the wrist. ROM has been similarly assessed in the human shoulder to study BPBI.³⁵ Differences between simulated and experimental ROM were quantified using percent error.

2.4 | Simulation

Animal-specific shoulder protraction and elbow flexion kinematic trajectories from gait analysis were used to simulate movement in the sagittal plane of the corresponding musculoskeletal model. Other degrees of freedom were set to zero. Muscle fiber length trajectories were extracted and normalized to optimal fiber length. Normalized fiber excursion was calculated as the difference between maximum and minimum normalized fiber lengths for a muscle. Normalized muscle fiber excursions were averaged by group and superimposed on a normalized force-length curve based on sarcomere lengths in literature³⁶ to estimate the operating

range of selected muscles during functional movement. The muscles selected for this analysis were those for which group-averaged optimal muscle length of the neurectomy-impaired limb was significantly shorter than that of the contralateral limb (biceps long head, biceps short head, pectoralis major, spinal deltoid, subscapularis, supraspinatus, and teres major).¹² These muscles were chosen to elucidate potential effects of restricted muscle growth on functional muscle fiber excursion.

2.5 | Statistical methods

A significance level of 0.05 and a confidence interval of 95% was used for all analyses of kinematic data and muscle fiber lengths. Where applicable, data were screened for normality with the Shapiro-Wilk test and visual inspection of QQ plots in GraphPad Prism (GraphPad Software). All other analyses were performed in MATLAB. The effect of injury location on duty factor was assessed using one-way analysis of variance (ANOVA) with Tukey post hoc analysis for pairwise group comparisons, and effect sizes were estimated using standardized mean differences corrected for small sample bias (Hedges's *d* statistic).³⁷ To evaluate the effect of injury location on limb posture, one-dimensional paired *t* test statistical parametric mapping (SPM) analyses were conducted on kinematics data. SPM, originally developed for neuroimaging to study time series data, permits presentation of statistical results in the original spatiotemporal spectra of the data.^{38–40} Previous work has demonstrated utility of SPM in analyzing kinematics time series data to identify temporal periods of differences in limb posture.⁴¹ In this study, SPM analyses incorporated SPM1D functions described by Pataky.⁴² Additionally, the relationship between animal-specific pairs of functional shoulder protraction ROM and passive shoulder external rotation ROM were assessed with linear regression.

After simulating gait in musculoskeletal models, the effect of injury location on individual muscles was studied using one-dimensional paired *t* test SPM analyses on time-series normalized fiber length data. The effect of injury location on normalized fiber excursion was investigated for each muscle actuator using one-way ANOVA, and effect sizes were estimated using Hedges's *d* statistic.

3 | RESULTS

3.1 | Muscle architecture

Muscle architecture parameters used to develop animal-specific musculoskeletal models are reported by group (mean \pm standard deviation) in Tables 1 and 2.

3.2 | Gait analysis

Limb posture extracted from gait analysis revealed less consistent kinematics (as quantified by standard deviation) for elbow flexion angles in neurectomy groups compared with control (Figure 3).

TABLE 1 Measured muscle fiber lengths (l^F); calculated optimal fiber lengths (l_o^F), physiological cross-sectional areas (PCSA), and maximum isometric forces (F_o^M); and simulated tendon slack lengths (l^{ST}) for muscles crossing the shoulder in unimpaired forelimbs of the control group

Muscle	Control				
	l^F (mm)	l_o^F (mm)	PCSA (mm ²)	F_o^M (N)	l^{ST} (mm)
Pectoralis major	15.58 ± 0.78	16.03 ± 1.27	19.16 ± 6.42	9.73 ± 3.26	7.5 ± 0.8
Anterior deltoid	9.74 ± 2.27	9.39 ± 1.96	13.75 ± 3.98	6.98 ± 2.02	3.7 ± 1.8
Spinal deltoid	9.66 ± 1.88	12.17 ± 2.47	10.46 ± 3.68	5.31 ± 1.87	7.7 ± 1.8
Biceps long head	10.57 ± 1.68	11.34 ± 1.94	8.48 ± 2.39	4.31 ± 1.22	19.4 ± 1.6
Biceps short head	9.86 ± 1.12	11.57 ± 1.54	1.21 ± 0.37	0.62 ± 0.19	16.9 ± 1
Subscapularis	8.59 ± 1.60	8.92 ± 1.37	29.75 ± 7.34	15.11 ± 3.73	10.5 ± 1.5
Supraspinatus	11.04 ± 1.81	10.15 ± 1.48	19.41 ± 3.98	9.86 ± 2.02	8.9 ± 1.8
Infraspinatus	10.68 ± 1.66	10.65 ± 1.60	20.07 ± 5.17	10.20 ± 2.62	7.0 ± 1.6
Teres major	10.70 ± 0.81	14.89 ± 0.87	13.11 ± 3.70	6.66 ± 1.88	8.7 ± 0.8
Triceps long head	10.15 ± 1.28	12.32 ± 1.83	55.33 ± 14.97	28.11 ± 7.60	12.8 ± 1.2

Note: Values represent mean ± standard deviation.

TABLE 2 Measured muscle fiber lengths (l^F); calculated optimal fiber lengths (l_o^F), physiological cross-sectional areas (PCSA), and maximum isometric forces (F_o^M); and simulated tendon slack lengths (l^{ST}) for muscles crossing the shoulder in affected forelimbs of the neurectomy groups

Muscle	l^F (mm)	l_o^F (mm)	PCSA (mm ²)	F_o^M (N)	l^{ST} (mm)
Preganglionic neurectomy					
Pectoralis major	15.19 ± 3.24	16.13 ± 4.56	16.97 ± 3.69	8.62 ± 1.87	7.9 ± 3.1
Anterior deltoid	6.56 ± 1.65	6.15 ± 1.75	6.11 ± 3.19	3.10 ± 1.62	6.6 ± 1.6
Spinal deltoid	9.17 ± 1.73	10.23 ± 1.59	4.82 ± 3.60	2.45 ± 1.83	8.2 ± 1.7
Biceps long head	9.79 ± 2.54	9.18 ± 2.85	3.72 ± 2.53	1.89 ± 1.28	20.2 ± 2.5
Biceps short head	8.85 ± 1.89	9.26 ± 2.59	1.66 ± 0.71	0.84 ± 0.36	17.8 ± 1.8
Subscapularis	9.48 ± 1.58	10.53 ± 2.93	10.81 ± 8.01	5.49 ± 4.07	9.6 ± 1.5
Supraspinatus	9.97 ± 2.04	9.26 ± 2.88	7.59 ± 9.05	3.86 ± 4.60	9.9 ± 2.0
Infraspinatus	9.89 ± 1.53	9.86 ± 1.48	5.36 ± 4.76	2.72 ± 2.42	7.9 ± 1.6
Teres major	10.64 ± 3.11	12.15 ± 3.62	7.77 ± 6.12	3.95 ± 3.11	8.7 ± 3
Triceps long head	9.17 ± 1.81	10.94 ± 2.28	52.03 ± 11.07	26.43 ± 5.62	13.7 ± 1.7
Postganglionic neurectomy					
Pectoralis major	14.11 ± 1.95	14.12 ± 1.67	11.78 ± 1.48	5.98 ± 0.75	8.9 ± 1.9
Anterior deltoid	6.15 ± 1.16	6.32 ± 1.04	11.24 ± 6.64	5.71 ± 3.38	7.0 ± 1.1
Spinal deltoid	7.96 ± 0.71	9.85 ± 1.24	5.60 ± 3.71	2.85 ± 1.88	9.2 ± 0.6
Biceps long head	8.44 ± 2.01	9.21 ± 2.11	3.74 ± 3.12	1.90 ± 1.58	21.6 ± 1.8
Biceps short head	9.60 ± 1.04	12.19 ± 2.5	2.16 ± 2.09	1.10 ± 1.06	17.0 ± 1.1
Subscapularis	7.24 ± 1.01	7.99 ± 1.07	19.32 ± 6.43	9.81 ± 3.27	11.7 ± 1.0
Supraspinatus	8.78 ± 1.28	9.09 ± 1.08	16.55 ± 5.48	8.41 ± 2.79	11.1 ± 1.2
Infraspinatus	10.16 ± 1.95	10.86 ± 1.61	13.87 ± 2.47	7.05 ± 1.26	7.5 ± 1.9
Teres major	9.88 ± 2.12	11.90 ± 2.43	7.93 ± 5.87	4.03 ± 2.98	9.5 ± 2.1
Triceps long head	8.47 ± 3.15	9.60 ± 3.17	28.94 ± 32.38	14.7 ± 16.45	14.4 ± 3.0

Note: Values represent mean ± standard deviation.

Differences in limb posture patterns were further explored through SPM, discussed below. Limb posture time series data were segmented into swing and stance phases before SPM, because duty factor differed significantly ($p = 0.00166$) across surgical intervention groups (Figure 4). Specifically, duty factor was lower ($p = .00116$), indicating reduced stance time on the limb, for the preganglionic neurectomy group (0.431 ± 0.094) compared with control (0.631 ± 0.049). Duty factor did not differ significantly for the postganglionic neurectomy group (0.533 ± 0.081) compared with control or preganglionic neurectomy groups. Duty factor data were normally distributed, and effect sizes (with 95% confidence intervals) were $d = -2.46 [-4.02, -0.90]$ between control and preganglionic neurectomy groups, $d = -1.35 [-2.62, -0.07]$ between control and postganglionic neurectomy groups, and $d = 1.07 [-0.15, 2.30]$ between preganglionic and postganglionic neurectomy groups.

SPM revealed that the preganglionic neurectomy group walked with less shoulder protraction and elbow flexion during late stance and early swing than did the control or postganglionic neurectomy groups (Figure 5). The preganglionic neurectomy group exhibited significantly less shoulder protraction than control (Figure 5A,B) in late stance ($p = 0.00890$) and just after toe-off in early swing phase ($p = 0.0488$). Similarly, the preganglionic neurectomy group exhibited significantly less elbow flexion than control (Figure 5C,D) in late stance just before toe-off ($p = 0.0498$), with this trend becoming more

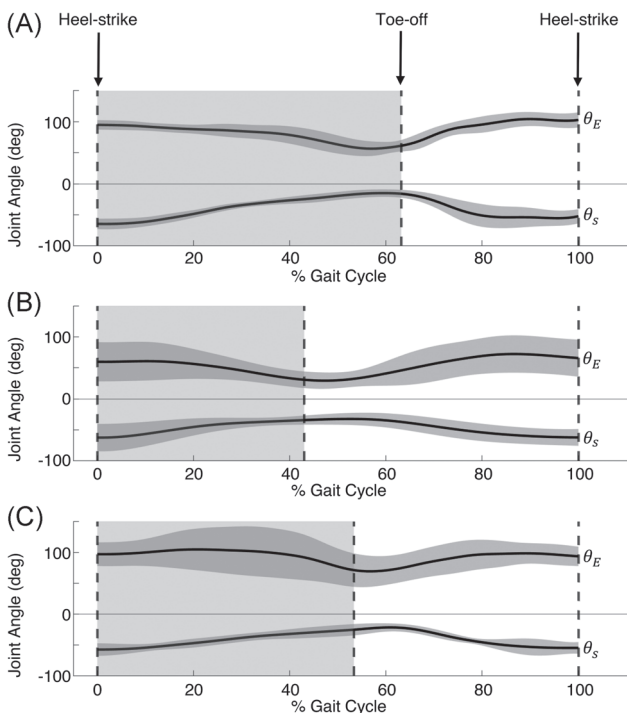


FIGURE 3 Average joint angle trajectories normalized to gait cycle for (A) control, (B) preganglionic neurectomy, and (C) postganglionic neurectomy groups. Mean joint angles (solid black lines) and standard deviations (dark gray bands) are shown for the shoulder (θ_s) and elbow (θ_E). Key gait events including heel strike and toe-off (dashed black lines), percent of time in stance (light gray regions) and percent time in swing (white regions) are highlighted

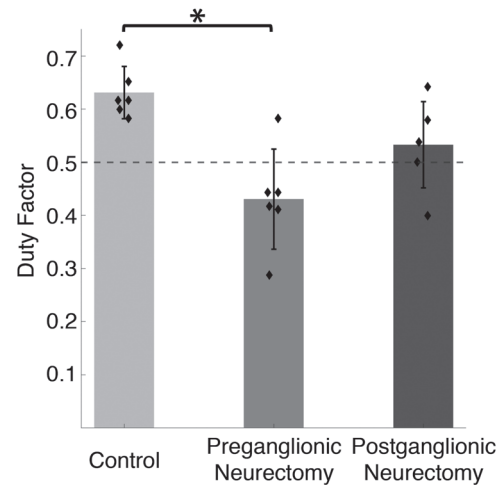


FIGURE 4 Mean duty factor, the fraction of the gait cycle spent in stance, by surgical intervention group. In able-bodied gait, walking should have a duty factor above 0.5 (dotted line). * $p < 0.05$

pronounced in early and mid-swing ($p < 0.001$), and presenting again at terminal swing ($p = 0.0399$). Comparison between neurectomy groups revealed that the preganglionic neurectomy group walked with less elbow flexion than did the postganglionic neurectomy group (Figure 5E,F). These differences, presenting in late stance ($p = 0.00220$) and early swing ($p = 0.00930$), were centered equally about toe-off. SPM did not detect significant differences in shoulder or elbow posture between the postganglionic neurectomy and control groups or in shoulder protraction between neurectomy groups.

ROM data were normally distributed. Linear regressions revealed that functional shoulder protraction ROM was not significantly related to passive external rotation ROM, either within surgical intervention groups (control: $r^2 = 0.182$, $p = 0.399$; preganglionic neurectomy: $r^2 = 0.399$, $p = 0.179$; postganglionic neurectomy: $r^2 = 0.122$, $p = 0.497$) or across groups combined ($r^2 = 0.0614$, $p = 0.322$) (Figure 6).

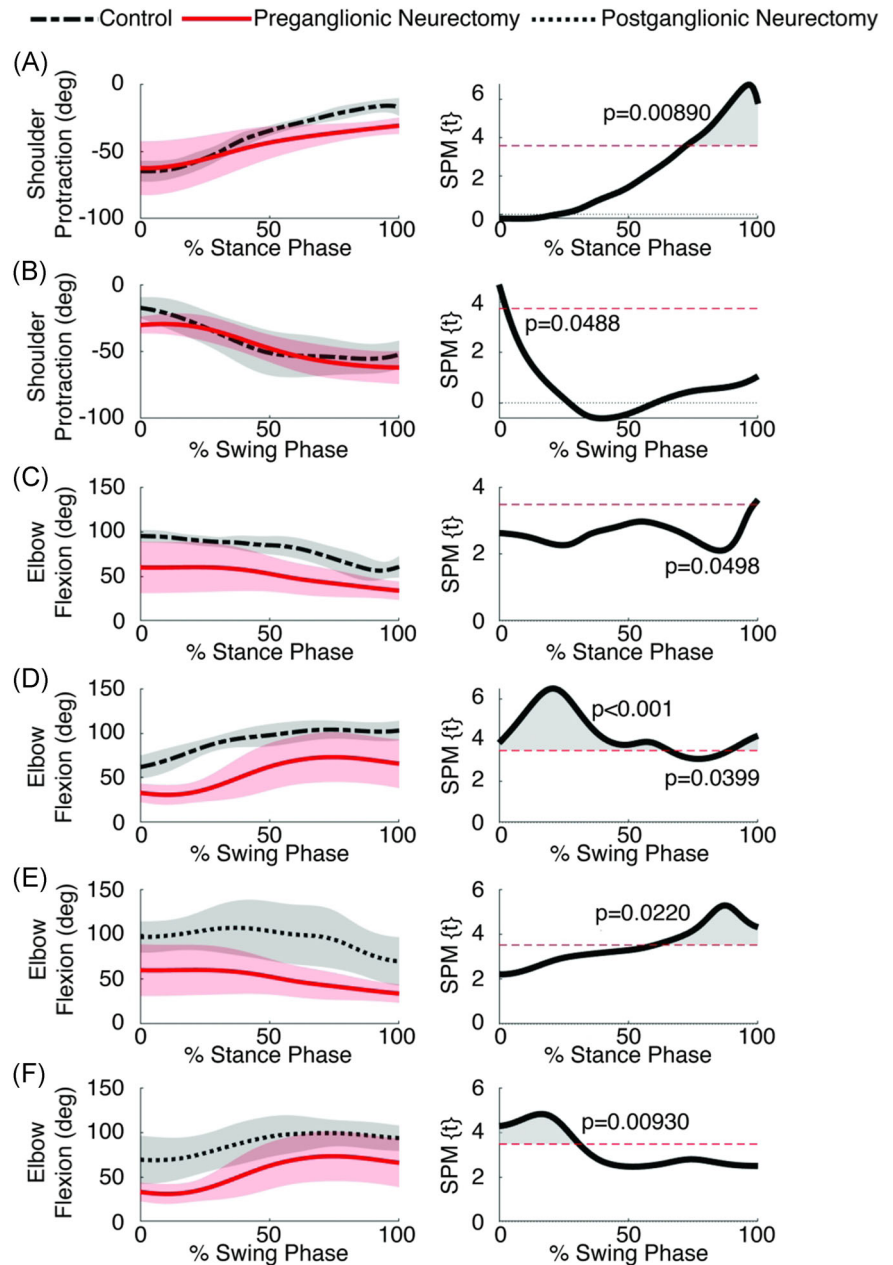
3.3 | Musculoskeletal model

The average passive shoulder external rotation predicted by musculoskeletal models of the unimpaired rat forelimb was 70.0° . Compared with the average experimental ROM¹⁸ for control animals (79.4°), error was 11.9%.

3.4 | Simulation

SPM on normalized fiber length trajectories revealed differences for only three of 14 modeled muscle actuators. The anterior deltoid had significantly shorter normalized fiber length trajectory throughout the gait cycle ($p < 0.001$) in the postganglionic neurectomy group compared with control. The biceps long head and triceps long head had significantly shorter normalized fiber length trajectories during portions of movement ($p = 0.0500$ briefly during swing phase for biceps long head; $p = 0.0427$ briefly

FIGURE 5 Sagittal plane joint angle trajectories during functional movement (left), with mean (lines) and standard deviation (shaded bands) of limb postures shown for stance and swing phases. *T*-value trajectories from SPM corresponding to joint angle trajectory plots (right); shaded areas indicate significant differences in limb posture, and dotted lines represent the significance threshold ($\alpha=0.05$). Limb posture differences are shown for control and preganglionic neurectomy groups at the shoulder (A,B) and elbow (C,D), and for preganglionic and postganglionic neurectomy groups at the elbow (E,F). SPM, statistical parametric mapping



during stance phase for triceps long head) in the preganglionic neurectomy group compared with control. SPM did not reveal differences in other muscles.

For most modeled muscle actuators, normalized muscle fiber excursions did not differ significantly between surgical intervention groups. Normalized muscle fiber excursion data were normally distributed, and only the triceps long head normalized fiber excursion differed significantly between surgical intervention groups ($p=0.00543$). Post hoc pairwise comparisons indicated that the triceps long head had shorter normalized fiber excursion in preganglionic (0.445 ± 0.123 , $p=0.0163$) and postganglionic neurectomy groups (0.432 ± 0.186 , $p=0.00990$) compared with control (0.632 ± 0.161), with medium effect sizes (Figure 7). Injury location had a small mean effect on excursion with confidence intervals containing zero for all other actuators (Figure 7).

Superimposition of muscle fiber excursions on a normalized force-length curve revealed that all muscles chosen for this analysis (except subscapularis) accessed regions of the curve that overlapped among surgical intervention groups (Figure 8).

4 | DISCUSSION

The objective of this study was to develop an integrated experimental and computational technique for measuring functional movement, and to investigate the effect of brachial plexus injury location on functional movement outcomes in a rat model of BPBI. To this end, we developed a musculoskeletal model of the rat forelimb, adapted the model to animal-specific muscle architecture parameters, and simulated locomotion using animal-specific limb posture

from gait analysis. We analyzed the effect of injury location on functional limb postures and functional use of muscles typically affected by BPBI.

Gait analysis revealed a more pronounced impact on limb posture following preganglionic brachial plexus injury than postganglionic injury. During both swing and stance, elbow flexion in rats with preganglionic neurectomy was smaller than that observed in control and postganglionic neurectomy groups. Reduced elbow flexion following preganglionic neurectomy is consistent with passive contractures observed in mouse models of BPBI.¹⁰ The effect of BPBI on shoulder movement is less straightforward: for the same rats, Dixit et al.¹² reported passive shoulder contracture following postganglionic neurectomy, whereas we only found significant functional differences following preganglionic neurectomy. The effect size of -1.35 $[-2.62, -0.07]$ for comparison of duty factor suggests that there may be a difference between control and post-

ganglionic neurectomy groups that this study was not powered to detect. Further investigation revealed no significant linear relationship between passive and functional shoulder ROM. We conclude that the passive external rotation shoulder ROM is not an effective predictor of functional shoulder protraction performance in rat models of BPBI. Across limb postures, differences due to preganglionic injury primarily presented during late-stance and early-swing (i.e., centered around toe-off). This coincides with the portion of gait where loads on the limb are highest. Given that rats with preganglionic neurectomy also spent significantly less time in stance, we suspect that altered shoulder movement patterns and reduced elbow flexion are compensatory mechanisms to manage limb loading following preganglionic injury. The existence of compensatory mechanisms might also explain the variability in kinematics seen in both neurectomy groups; individual strategies to manage limb loading would result in less consistent joint kinematics for the group, especially at the elbow.

The more pronounced impact on limb posture following preganglionic neurectomy is consistent with the more severe alterations to muscle architecture following this injury.¹² A study reporting qualitative changes to limb posture following preganglionic BPBI consistent with those observed in this study attributed the observed changes to weakness of the shoulder and forelimb, as motor coordination was found to be unimpaired.⁸ For passive movement, shoulder internal rotation and elbow flexion contractures have frequently been attributed to impaired longitudinal muscle growth.¹⁰ However, we found that normalized muscle fiber excursions did not differ significantly between surgical intervention groups, even in muscles for which longitudinal muscle growth was significantly restricted, as documented by reduced optimal muscle length in the neurectomy-impaired limb compared with the contralateral limb.¹² Further investigation revealed that when superimposed on a

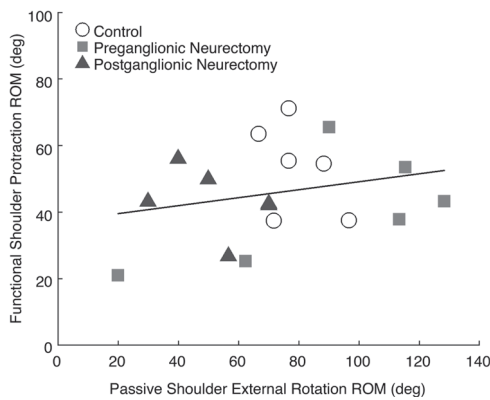


FIGURE 6 Linear regression between functional shoulder protraction and passive shoulder external rotation range of motion (ROM) across animals. $r^2 = 0.0614$, slope $p = 0.322$

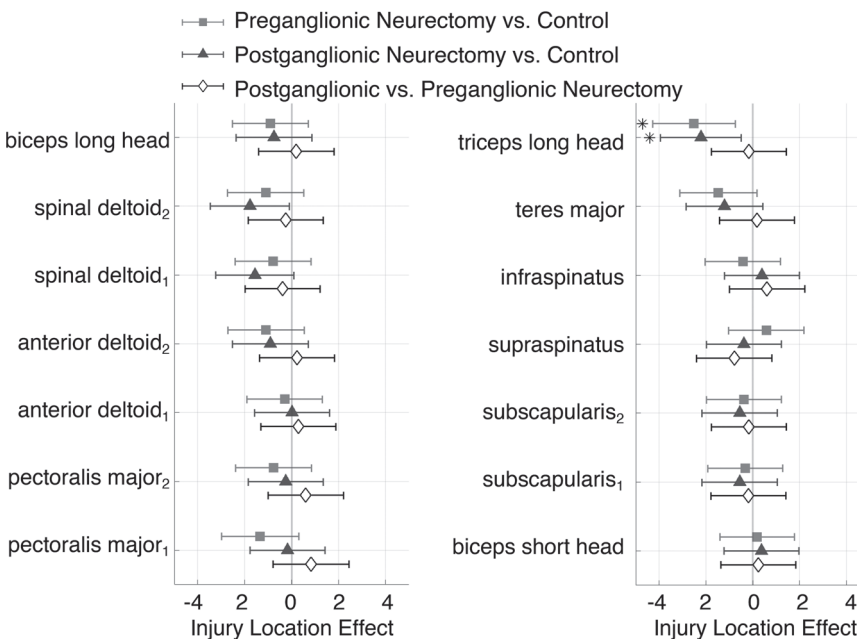
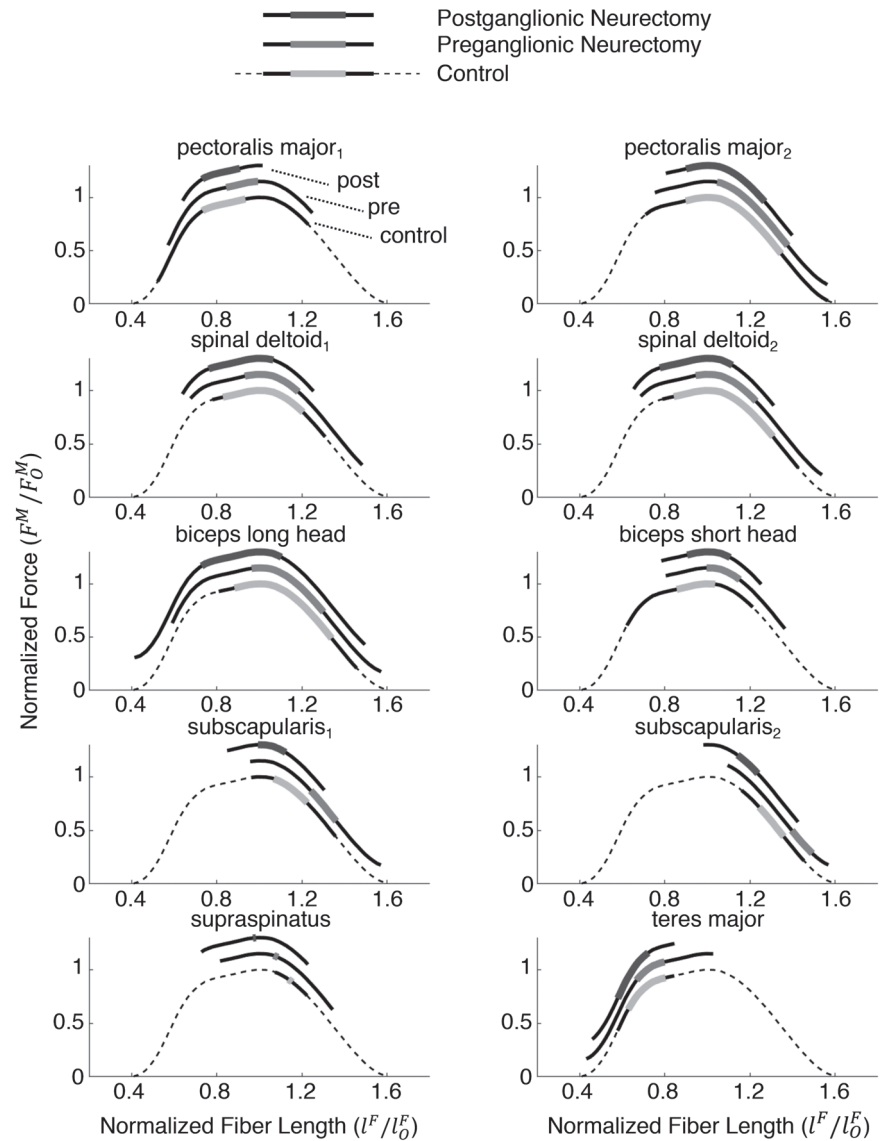


FIGURE 7 Effect sizes with 95% confidence intervals for the effect of injury location on normalized muscle fiber excursions, estimated using Hedges's d statistic. Negative effect sizes indicate that the treatment (listed as the former of the comparison) had a lower mean normalized muscle fiber excursion. $*p < 0.05$

FIGURE 8 Functional movement excursions averaged by group and superimposed on normalized force-length curves. Dotted black lines represent the normalized force-length curve based on sarcomere lengths in literature.³⁶ Stacked, solid gray lines represent the group-averaged range of normalized muscle fiber lengths during a single gait cycle (bottom: control; middle: preganglionic; top: postganglionic). Solid black lines represent standard deviations. Ten muscle-tendon actuators represent seven muscles for which the group-averaged optimal muscle length of the neurectomy-impaired limb was significantly shorter than that of the contralateral limb



normalized force-length curve, most neurectomy-impaired muscle fibers with these significant optimal muscle length differences accessed regions of the normalized force-length curve that overlapped with the control group.¹² Given that functional limb postures are clearly different following BPBI, these differences likely reflect compensatory mechanisms employed during locomotion to retain consistent access to muscle excursion regions. Altered joint angle patterns in impaired animals may be strategic to achieve stable gait or comfort. We conclude that the observed differences in functional limb posture are not dictated by altered muscle architecture alone, but rather a result of the coupled effects of altered muscle architecture and altered motor control strategy. Our findings suggest the likely presence of compensatory motor control strategies during locomotion following BPBI.

Considering the effect of BPBI on the central nervous system is important for contextualizing the notion of altered motor control. Studies in human patients have demonstrated significant neuroplastic changes following birth and traumatic brachial plexus injuries.⁴³

In young BPBI patients, use of the affected hand was found to elicit more sensorimotor cortex activity than use of the unaffected hand, suggesting recruitment of contralateral pathways as compensation for ipsilateral developmental disruption.⁴⁴ Interestingly, cortical activity in associative motor regions was weaker in adult BPBI patients when observing able-bodied subjects performing actions; this protocol eliminates compensatory muscle activation.⁴⁵ Similarly, the supplementary motor area of adult brachial plexus injury patients displayed nearly no activation during motor imagery tasks involving fingers of the affected limb.⁴⁶ These patterns might suggest that when the affected limb is in use, there is neural compensation that is otherwise absent during observation or imagery tasks. These patterns of cortical reorganization further support the notion that compensatory motor control may play a role in rat gait following BPBI. Damage to the brachial plexus may also involve remodeling of the spinal cord and peripheral sensory pathways; further investigation, in both animal models and human patients, into the activation of muscles crossing the shoulder during functional movement and the effect of

injury on sensory pathways may elucidate the mechanisms dictating motor control following BPBI.

An important exception to the observed trend of overlapping excursions noted above is the subscapularis. The subscapularis plays an important role in elevation and internal rotation of the shoulder,^{47,48} and subscapularis impairment is considered a main contributor to passive shoulder contracture.^{9,10} Our results indicate that this muscle is affected both architecturally and functionally by BPBI. Appearance of subscapularis excursions on the descending region of the normalized force-length curve suggests a severity in subscapularis atrophy that makes the muscle particularly amenable to stretching.

The clinical implications of our findings support emphasis on movement analysis during functional tasks in treating BPBI. Following diagnosis, initial management of BPBI (at 2–3 weeks of age) typically comprises passive exercises aimed at preventing contracture and cortically reintegrating the affected limb.^{49,50} In follow-up visits, infants are assessed for spontaneous biceps recovery, internal rotation contracture, and glenohumeral congruency.⁴⁹ In typical cases of spontaneous biceps recovery at 3 months of age, conservative treatment methods (such as passive and active mobilization exercises, sensory stimulation, and bimanual activities) are employed in place of surgery.⁵⁰ While further outcome assessment encompasses numerous methods, documented consensus is that ROM should be measured for passive and active joint movement and the Mallet score (which evaluates five functional movements) should be determined.⁵¹ It has been noted that as infants with BPBI gain intentional voluntary control, they may experience “learned non-use” of the affected side; they rely on contralateral capabilities even when ipsilateral function improves over time.⁴⁴ Emphasis on complex functional tasks in therapy may optimize cortical reintegration of the affected limb. Given that passive functionality may not be an effective predictor of functional performance, functional movement analysis may reveal information that passive outcomes alone cannot. Furthermore, the observed variability in individual kinematics coupled with the likely presence of compensatory motor control strategies following BPBI suggest that clinical evaluation of functional performance during complex functional tasks can elucidate mechanisms contributing to individual neuromotor and musculoskeletal deficits. Finally, given that functional ROM determines joint loading and subsequent joint development, our findings support existing therapeutic and assessment strategies that focus on restoration of functional ROM in addition to passive ROM.

Limitations of this study should be considered. Muscle pennation angle, set to zero due to its minimal effect on PCSA,³¹ may affect fiber excursion. For comparison of the same muscles between surgical intervention groups, however, we considered this effect negligible. Limb posture extraction and simulation was done in a single plane; although limited movement of the unimpaired rat forelimb has been documented in other planes during locomotion,²⁹ three-dimensional functional movement analysis may be advantageous in future studies. Identification of the shoulder rotation center during gait analysis can be challenging due to skin and other tissues,

which may introduce error in limb posture measurements. However, movement of the limb in gait videos more clearly reveals the center of rotation than is apparent from a static frame. Our analysis was performed 8 weeks postnatally, at which point deformity is well-established.¹⁹ Musculoskeletal deformities associated with BPBI progress with age,¹³ and injury location is known to have an effect on recovery⁷; future studies will evaluate functional performance at multiple postnatal time points. While individual muscle architecture measurements are reflected in the musculoskeletal models developed in this study, the same, unimpaired skeletal structure was used for all models: models were neither scaled to represent individual limb lengths nor adjusted to account for glenohumeral deformation introduced by BPBI. Future studies should consider the coupled effects of muscular and osseous deformities. Muscle fiber excursions were calculated using joint kinematics and muscle length properties; force production properties of muscles were not considered, and passive forces reflected here may underestimate the true value. Force production is important when considering joint loading during functional movement. Finally, differences between rodent and human shoulder anatomies must be considered when translating results to clinical applications. While musculoskeletal response to BPBI is very similar in rodent and human shoulders,^{9,13} this response is not identical. The rat shoulder is permanently weight-bearing whereas the human shoulder is only weight-bearing during the first year of life, when infants crawl. However, our previous work has demonstrated that computational rodent models simulated with experimental data reproduce loading orientations and muscle behaviors observed in computational human models of BPBI simulated with clinical data. Furthermore, simulations in rodent BPBI models of glenohumeral development using these joint loads to directly drive simulated bone growth predict rat glenoid morphology that both replicates experimental micro-CT scans and results in deformities similar to those observed in humans.^{35,52,53}

The key contributions of this study are the development of a musculoskeletal model of the rat forelimb and detailed insight into the effects of preganglionic and postganglionic BPBI on functional limb movement. This study offers new information regarding the effect of injury location on limb posture during locomotion. Our findings suggest that compensatory motor control strategies may account for significant changes to functional outcomes following BPBI. Our noninvasive framework integrating musculoskeletal modeling with gait analysis to identify temporal regions of significant differences can be extended to assess the progression of injury and recovery, as well as the effectiveness of treatments for BPBI, among other upper limb neuromusculoskeletal injuries.

ACKNOWLEDGMENTS

The authors would like to thank Emily Keller for assistance with development of the musculoskeletal models. This study is supported by the National Institutes of Health grant R21 HD088893.

CONFLICT OF INTERESTS

The authors declare that there are no conflict of interests.

AUTHOR CONTRIBUTIONS

Raveena M. Doshi contributed to study design, performed data acquisition and analysis, drafted the paper, and approved the paper for submission. Monique Y. Reid, Nikhil N. Dixit, and Emily B. Fawcett performed data acquisition and approved the paper for submission. Jacqueline H. Cole contributed to study design, critically revised the paper, and approved the paper for submission. Katherine R. Saul developed the study design, contributed to interpretation of the data, critically revised the paper, and approved the paper for submission. All authors have read and approved the final submitted manuscript.

ORCID

Raveena M. Doshi  <http://orcid.org/0000-0002-1378-4620>

Nikhil N. Dixit  <http://orcid.org/0000-0002-8876-4819>

Jacqueline H. Cole  <https://orcid.org/0000-0002-0233-9425>

Katherine R. Saul  <https://orcid.org/0000-0002-8439-7951>

REFERENCES

- Foad SL, Mehlman CT, Ying J. The epidemiology of neonatal brachial plexus palsy in the United States. *J Bone Joint Surg Am.* 2008;90:1258-1264.
- Lagerkvist AL, Johansson U, Johansson A, Bager B, Uvebrant P. Obstetric brachial plexus palsy: a prospective, population-based study of incidence, recovery, and residual impairment at 18 months of age. *Dev Med Child Neurol.* 2010;52:529-534.
- Pearl ML. Shoulder problems in children with brachial plexus birth palsy: evaluation and management. *J Am Acad Orthop Surg.* 2009;17:242-254.
- Pondaag W, Malessy MJ, van Dijk JG, Thomeer RT. Natural history of obstetric brachial plexus palsy: a systematic review. *Dev Med Child Neurol.* 2004;46:138-144.
- Nikolaou S, Hu L, Cornwall R. Afferent innervation, muscle spindles, and contractures following neonatal brachial plexus injury in a mouse model. *J Hand Surg Am.* 2015;40:2007-2016.
- Al-Qattan MM. Obstetric brachial plexus palsy associated with breech delivery. *Ann Plast Surg.* 2003;51:257-264.
- Ferrante MA. Brachial plexopathies: classification, causes, and consequences. *Muscle Nerve.* 2004;30:547-568.
- Ochiai H, Ikeda T, Mishima K, et al. Development of a novel experimental rat model for neonatal preganglionic upper brachial plexus injury. *J Neurosci Methods.* 2002;119:51-57.
- Soldado F, Benito-Castillo D, Fontecha CG, et al. Muscular and glenohumeral changes in the shoulder after brachial plexus birth palsy: an MRI study in a rat model. *J Brachial Plex Peripher Nerve Inj.* 2012;7:9.
- Nikolaou S, Peterson E, Kim A, Wylie C, Cornwall R. Impaired growth of denervated muscle contributes to contracture formation following neonatal brachial plexus injury. *J Bone Joint Surg Am.* 2011;93:461-470.
- Crouch DL, Hutchinson ID, Plate JF, et al. Biomechanical basis of shoulder osseous deformity and contracture in a rat model of brachial plexus birth palsy. *J Bone Joint Surg Am.* 2015;97:1264-1271.
- Dixit NN, McCormick CM, Warren E, Cole JH, Saul KR. Preganglionic and postganglionic brachial plexus birth injury effects on shoulder muscle growth. *J Hand Surg Am.* 2020;46:146.e1-146.e9. <https://pubmed.ncbi.nlm.nih.gov/32919794/>
- Kim HM, Galatz LM, Das R, Patel N, Thomopoulos S. Musculoskeletal deformities secondary to neurotomy of the superior trunk of the brachial plexus in neonatal mice. *J Orthop Res.* 2010;28:1391-1398.
- Hennen K, Crouch DL, Hutchinson ID, Li Z, Saul KR. Relationship between glenoid deformity and gait characteristics in a rat model of neonatal brachial plexus injury. *J Orthop Res.* 2018;36:1991-1997.
- Holzbaumer KRS, Murray WM, Delp SL. A model of the upper extremity for simulating musculoskeletal surgery and analyzing neuromuscular control. *Ann Biomed Eng.* 2005;33:829-840.
- Garner BA, Pandey MG. Musculoskeletal model of the upper limb based on the visible human male dataset. *Comput Methods Biomech Biomed Eng.* 2001;4:93-126.
- Johnson WL, Jindrich DL, Roy RR, Reggie, Edgerton V. A three-dimensional model of the rat hindlimb: musculoskeletal geometry and muscle moment arms. *J Biomech.* 2008;41:610-619.
- Dixit NN, McCormick C, Warren E, et al. Preganglionic and postganglionic neonatal brachial plexus injury effects on muscle properties and range of motion. In: Orthopaedic Research Society Annual Meeting, New Orleans, LA. 2018;10-13. Available from: <http://www.ors.org/Transactions/64/O635.pdf>
- Quinn R. Comparing rat's to human's age: how old is my rat in people years? *Nutr.* 2005;21:775-777.
- Burkholder TJ, Lieber RL. Sarcomere length operating range of vertebrate muscles during movement. *J Exp Biol.* 2001;204:1529-1536.
- Mendez J, Keys A. Density and composition of mammalian muscle. *Metabolism.* 1960;9:184-188.
- Sacks RD, Roy RR. Architecture of the hind limb muscles of cats: Functional significance. *J Morphol.* 1982;173:185-19.
- Saul KR, Hu X, Goehler CM, et al. Benchmarking of dynamic simulation predictions in two software platforms using an upper limb musculoskeletal model. *Comput Methods Biomech Biomed Eng.* 2015;18:1445-1458.
- Shimada H, Hamakawa M, Ishida A, Tamakoshi K, Nakashima H, Ishida K. Low-speed treadmill running exercise improves memory function after transient middle cerebral artery occlusion in rats. *Behav Brain Res.* 2013;243:21-27.
- Nishioka R, Sugimoto K, Aono H, et al. Treadmill exercise ameliorates ischemia-induced brain edema while suppressing Na⁺/H⁺ exchanger 1 expression. *Exp Neurol.* 2016;277:150-161.
- Leblond H, L'Espérance M, Orsal D, Rossignol S. Treadmill locomotion in the intact and spinal mouse. *J Neurosci.* 2003;23:11411-11419.
- Delp SL, Anderson FC, Arnold AS, et al. OpenSim: open-source software to create and analyze dynamic simulations of movement. *IEEE Trans Biomed Eng.* 2007;54:1940-1950.
- Seth A, Hicks JL, Uchida TK, et al. OpenSim: simulating musculoskeletal dynamics and neuromuscular control to study human and animal movement. *PLoS Comput Biol.* 2018;14:e1006223.
- Bonnan MF, Shulman J, Varadarajan R, et al. Forelimb kinematics of rats using XROMM, with implications for small eutherians and their fossil relatives. *PLoS One.* 2016;11:1-21.
- Zajac FE. Muscle and tendon: properties, models, scaling, and application to biomechanics and motor control. *Crit Rev Biomed Eng.* 1989;17:359-411.
- Swan MA, Sato E, Galatz LM, Thomopoulos S, Ward SR. The effect of age on rat rotator cuff muscle architecture. *J Shoulder Elbow Surg.* 2014;23:1786-1791.
- Greene EC. *Anatomy of the rat.* New York: Hafner Pub; 1963.
- Bohensky F. *Photo Manual & Dissection Guide of the Rat: With Sheep Eye.* New York: Square One Education Guides; 2004.
- Dyce KM, Sack WO, Wensing CJG. *Textbook of veterinary anatomy. Saunders/.* Elsevier; 2010.
- Cheng W, Cornwall R, Crouch DL, Li Z, Saul KR. Contributions of muscle imbalance and impaired growth to postural and osseous shoulder deformity following brachial plexus birth palsy: a computational simulation analysis. *J Hand Surg Am.* 2015;40:1170-1176.

36. Murray WM, Buchanan TS, Delp SL. The isometric functional capacity of muscles that cross the elbow. *J Biomech.* 2000;33:943-952.
37. Hedges LV, Olkin I. *Statistical Methods for Meta-Analysis.* Orlando: Academic Press; 1985.
38. Pataky TC. Generalized n-dimensional biomechanical field analysis using statistical parametric mapping. *J Biomech.* 2010;43:1976-1982.
39. Pataky TC. One-dimensional statistical parametric mapping in Python. *Comput Methods Biomech Biomed Engin.* 2012;15:295-301.
40. Pataky TC, Robinson MA, Vanrenterghem J. Vector field statistical analysis of kinematic and force trajectories. *J Biomech.* 2013;46:2394-2401.
41. Li X, Santago AC, Vidt ME, Saul KR. Analysis of effects of loading and postural demands on upper limb reaching in older adults using statistical parametric mapping. *J Biomech.* 2016;49:2806-2816.
42. Pataky TC. 2014. SPM1D. <http://www.spm1d.org/index.html>
43. Thaploo D, Bhat DI, Kulkarni MV, Devi BI. Brachial plexus injury and resting-state fMRI: need for consensus. *Neurol India.* 2019;67:679-683.
44. Longo E, Nishiyori R, Cruz T, Alter K, Damiano DL. Obstetric brachial plexus palsy: can a unilateral birth onset peripheral injury significantly affect brain development? *Dev Neurorehabilit.* 2020;23:375-382.
45. Tuna Z, Oskay D, Algin O, Koçak OM. Cortical motor areas show different reorganizational changes in adult patients with brachial plexus birth injury (BPBI). *Intl J Dev Neurosci.* 2020;80:389-395.
46. Lu YC, Liu HQ, Hua XY, et al. Supplementary motor area deactivation impacts the recovery of hand function from severe peripheral nerve injury. *Neural Reg Res.* 2016;11:670-675.
47. Otis JC, Jiang CC, Wickiewicz TL, Peterson MG, Warren RF, Santner TJ. Changes in the moment arms of the rotator cuff and deltoid muscles with abduction and rotation. *J Bone Joint Surg Am.* 1994;76:667-676.
48. Kuechle DK, Newman SR, Itoi E, Niebur GL, Morrey BF, An KN. The relevance of the moment arm of shoulder muscles with respect to axial rotation of the glenohumeral joint in four positions. *Clin Biomech.* 2000;15:322-329.
49. Thatte MR, Nayak NS, Hiremath AS. Management of birth brachial plexus injury including use of distal nerve transfers. *J Hand Surg Asian Pac.* 2020;25:267-275.
50. Frade F, Gómez-Salgado J, Jacobsohn L, Florindo-Silva F. Rehabilitation of neonatal brachial plexus palsy: integrative literature review. *J Clin Med.* 2019;8:980.
51. Pondaag W, Malessy MJA. Outcome assessment for brachial plexus birth injury. Results from the iPluto world-wide consensus survey. *J Orthop Res.* 2018;36:2533-2541.
52. Crouch DL, Plate JF, Li Z, Saul KR. Computational sensitivity analysis to identify muscles that can mechanically contribute to shoulder deformity following brachial plexus birth palsy. *J Hand Surg.* 2014; 39:303-311.
53. Dixit NN, McFarland DC, Fisher MB, Cole JH, Saul KR. Integrated iterative musculoskeletal modeling predicts bone morphology following brachial plexus birth injury (BPBI). *J Biomech.* 2020;103: 109658.

How to cite this article: Doshi RM, Reid MY, Dixit NN, Fawcett EB, Cole JH, Saul KR. Location of brachial plexus birth injury affects functional outcomes in a rat model. *J Orthop Res.* 2021;1-12. <https://doi.org/10.1002/jor.25173>